Experimental study of flash flood surges down a rough sloping channel

H. Chanson

Fluid Mechanics, Hydraulics and Environmental Engineering, Department of Civil Engineering, University of Queensland, Brisbane, Queensland, Australia

Received 7 September 2003; revised 17 December 2003; accepted 22 January 2004; published 16 March 2004.

[1] Flood waves resulting from flash floods and natural dam overtopping have been responsible for numerous losses. In the present study, surging waters down a flat stepped waterway ($\theta = 3.4°$) were investigated in a 24 m long chute. Wave front propagation data were successfully compared with *Hunt*'s [1982, 1984] theory. Visual observations highlighted strong aeration of the leading edge. Instantaneous distributions of void fractions showed a marked change in shape for $(t - t_s)*\sqrt{g/d_o} \sim 1.3$, which may be caused by some major differences between the wave leading edge and the flow behind, including nonhydrostatic pressure distributions, plug-slug flow regime, and different boundary friction regime. Practically, the results quantified the large amount of entrained air (i.e., ''white waters'') at the wave front, which in turn, reduces buoyancy and could affect sediment motion at the leading edge because the sediment relative density is inversely proportional to the entrained air content. *INDEX TERMS:* 1860 Hydrology: Runoff and streamflow; 1815 Hydrology: Erosion and sedimentation; 1821 Hydrology: Floods; 1894 Hydrology: Instruments and techniques; *KEYWORDS:* flash flood propagation, unsteady open channel flow, boundary friction, air-water flow, sediment motion

Citation: Chanson, H. (2004), Experimental study of flash flood surges down a rough sloping channel, *Water Resour. Res.*, *40*, W03301, doi:10.1029/2003WR002662.

1. Introduction

[2] Flood waves resulting from flash floods have been responsible for numerous damage and losses of life. For example, during an intense rainfall in southeast Queensland on 9 March 2001, severe flash flooding caused up to $20 millions of damage in the Brisbane area and two people drowned in separate incidents in floodwaters. Most rainfall occurred in less than 1 hour and the flash flood front propagated like a surge. *Bornschein and Pohl* [2003] documented a dam break which induced a flash flood surging through the streets of the Glashütte township, Germany. A related case of flash floods is the flooding of valley during armed conflicts: e.g., by the Assyrians (Babylon, Iraq BC 689), the Spartans (Mantinea, Greece BC 385-84), the Chinese (Huai river, AD 514-15), the Russian army (Dnieprostroy dam, 1941), by the Royal Air Force (Möhne dam, 1943) [*Ré*, 1946; *Dressler*, 1952; *Smith*, 1971; *Schnitter*, 1994].

[3] *Capart and Young* [1998] studied dam break wave propagation in movable bed laboratory flumes. They observed intense scouring of the bed at the leading edge of the bore. *Khan et al.* [2000] studied the effects of floating debris on dam break waves in laboratory also. Their results showed an accumulation of debris near the wave front and a reduction of the front celerity both with and without initial water levels. Despite few earlier studies (e.g., Table 1), current knowledge of flash flood surging down rough sloping waterways is still rudimentary. No robust surge prediction model has been developed for very-rough channels. Further photographs and video movies demonstrated the aerated nature of the advancing front [*Dressler*, 1954; *Baker*, 1994; *Bornschein and Pohl*, 2003], but this aspect remains totally unknown and unquantified. During the present study, flash flood surges were investigated in a large size stepped chute ($\theta = 3.4°$, 24 m long). The results provide new information on the rate of energy dissipation and on the downstream wave celerity. Unsteady two-phase flow measurements were further conducted in the wave front to comprehend the air-water flow structure and possible effects on debris and sediment motion.

[4] Considering the dam break wave down a smooth sloping channel, the kinematic wave approximation of the Saint-Venant equations may be solved analytically [*Hunt*, 1982]. For a prismatic rectangular channel, Hunt's analysis gives

$$\frac{V_H*S_o*t}{d_o} = \frac{1 - \left(\frac{d_s}{d_o}\right)^2}{\left(\frac{d_s}{d_o}\right)^{3/2}} \quad (1)$$

$$\frac{S_o*x_s}{d_o} = \frac{\frac{3}{2}}{\frac{d_s}{d_o}} - \frac{1}{2}*\frac{d_s}{d_o} - 1 \quad (2)$$

$$\frac{U}{V_H} = -\frac{3}{4}*\frac{V_H*S_o*t}{d_o} + \sqrt{\frac{S_o*x_s + d_o}{d_o} + \left(\frac{3}{4}*\frac{V_H*S_o*t}{d_o}\right)^2} \quad (3)$$

0043-1397/04/2003WR002662$09.00

Table 1. Summary of Surge Experiments and Observations Down Very Rough Channels[a]

Experiment	Θ, deg	h, m	Q(t = 0+), m^3/s	Initial Channel Condition	d_o, m	Remarks
Present study						
Series 1	3.4	0.143	0.019	empty	0.12	10 horizontal steps (l = 2.4 m).
	3.4	0.143	0.030	empty	0.161	W = 0.5 m. Nozzle depth: 0.030 m.
	3.4	0.143	0.040	empty	0.195	
	3.4	0.143	0.075	empty	0.30	
Series 2	3.4	0.0715	0.040	empty	0.195	18 horizontal steps (l = 1.2 m).
	3.4	0.0715	0.0475	empty	0.219	W = 0.5 m. Nozzle depth: 0.030 m.
	3.4	0.0715	0.055	empty	0.241	Air-water flow measurements conducted for
	3.4	0.0715	0.065	empty	0.270	Q(t = 0+) = 0.04, 0.055 & 0.075 m^3/s on
	3.4	0.0715	0.075	empty	0.300	steps 10 and 17.
Dressler (1954)	0	0.0056	0.0027	empty	0.055	65-m long horizontal channel with strip
	0	0.0056	0.0076	empty	0.11	roughness (h = 0.0056 m, l = 0.0224 m).
	0	0.0056	0.0215	empty	0.22	W = 0.225 m.
Brushes Clough dam spillway [*Baker*, 1994]	18.4	0.19	0.5	empty	~0.4	Prototype spillway. Inclined downward steps, trapezoidal channel (2 m bottom width). Data analysis by the author [*Chanson*, 2001].
Flash flood through Glashütte, Germany [*Bornschein and Pohl*, 2003]	–	–	–	wet	–	Flash flood caused by the flood retention Glashütte dam breach on 12 Aug. 2002 between 4:10 and 4:40pm. Video observations.

where t is the time with t = 0 at dam break, d_s is the dam break wave front thickness, x_s is the dam break wave front position measured from the dam site, U is the wave front celerity, d_o is the reservoir height at dam site, and S_o is the bed slope. (Note that the reservoir length is d_o/S_o.) The velocity V_H is the uniform equilibrium flow velocity for a water depth d_o:

$$V_H = \sqrt{\frac{8*g}{f}*d_o*S_o} \quad (4)$$

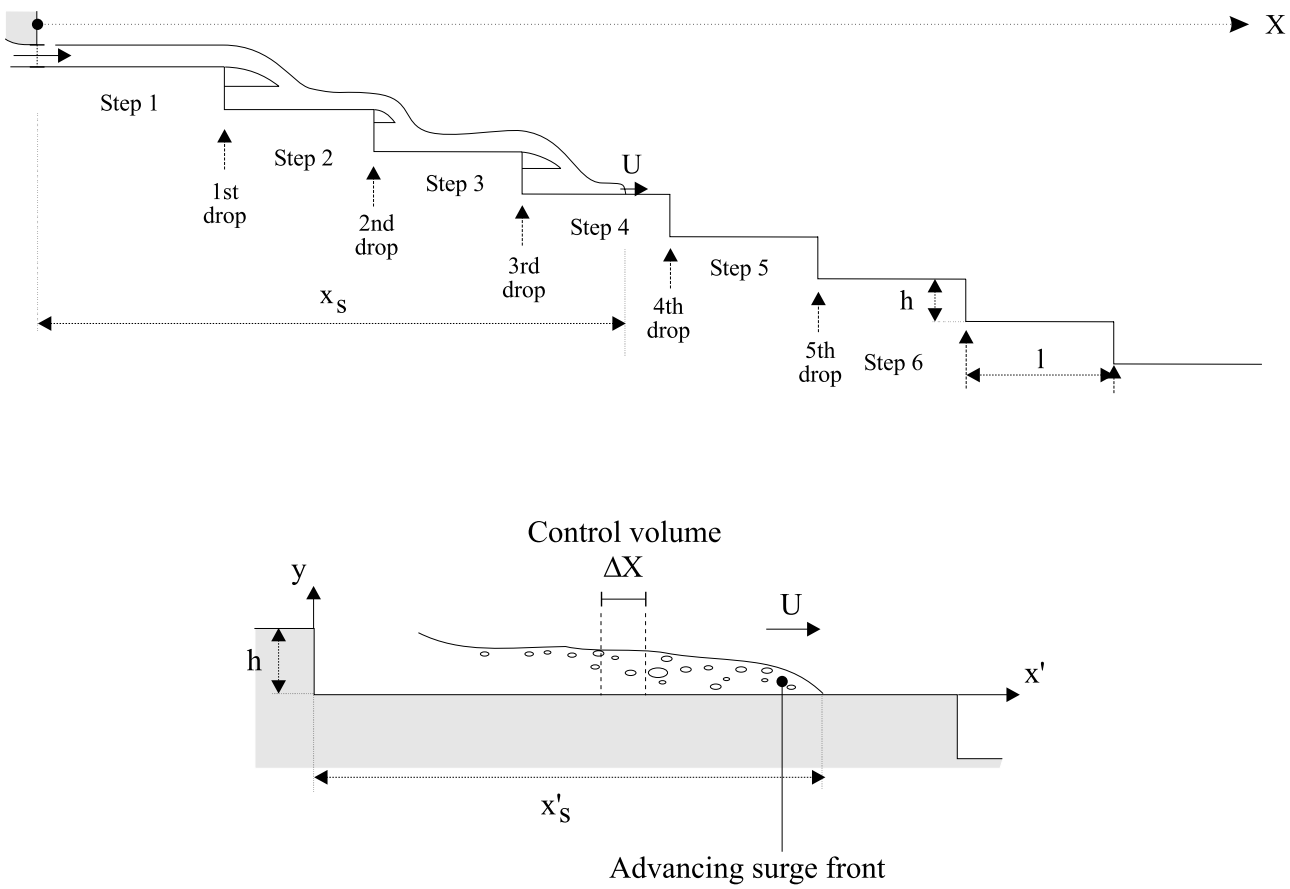

Figure 1a. Experimental facility at the University of Queensland: Definition sketch.

Figure 1b. Experimental facility at the University of Queensland: Experiment series 2 ($Q(t = 0+) = 0.065$ m^3/s, step 10, h = 0.0715 m). Surge front taking off, flow direction from top left to bottom right. Note the "white waters" at the leading edge. See color version of this figure in the HTML.

where g is the gravity acceleration and f is the Darcy friction factor which is assumed constant. Equations (1) to (4) are valid once the dam break wave has traveled more than 4 times the reservoir length and that the free surface is parallel to the bottom of the sloping channel. Equation (2) may be transformed:

$$\frac{d_s}{d_o} = \frac{3}{2} * \frac{d_o}{S_o * x_s - d_o} \quad \text{for } S_o * x_s / d_o > 4 \qquad (2')$$

Hunt [1984] developed further an analytical expression of the shock front shape:

$$\frac{S_o * (x - x_s)}{d_o} = \frac{d_s}{d_o} * \left(\frac{d}{d_s} + \text{Ln}\left(1 - \frac{d}{d_s}\right) + \frac{1}{2} \right) \qquad (5)$$

where d is the depth (or thickness) measured normal to the bottom.

[5] The elegant development of *Hunt* [1982, 1984] was verified by several series of experiments [e.g., *Hunt*, 1982, 1984; *Nsom et al.*, 2000].

2. Experimental Apparatus

[6] Experiments were performed in a 24 m long 0.5 m wide flume (Figures 1a and 1b). The channel slope was $S_o \approx 0.065$ (i.e., $\theta = 3.4°$). The flow rate was delivered by a pump controlled with an adjustable frequency AC motor drive Taian T-Verter K1/N1 (Pulse Width Modulated design), enabling an accurate discharge adjustment in a closed-circuit system. The flow was fed through a smooth convergent nozzle (1.7 m long), and the nozzle exit was 30 mm high and 0.5 m wide. Bed roughness was artificially generated by two stepped configurations detailed in Table 1. Two relevant studies are further listed in Table 1.

[7] In steady flow conditions, flow rates were measured with a Dall™ tube flowmeter, calibrated on site with a sharp-crested weir. The accuracy on the discharge measurement was about 2%. The surging flow was studied with high-shutter speed still- and video-cameras: i.e., a VHS video-camera Panasonic™ NV-RX10A (speed: 25 frames/sec., shutter: sport mode, zoom: 1 to 14), a digital video-camera handycam Sony™ DV-CCD DCR-TRV900 (speed: 25 fr/s, shutter: 1/4 to 1/10,000 sec., zoom: 1 to 48) and a digital camera Olympus™ Camedia C-700 (shutter: 1/2 to 1/1,000 sec., zoom: 1 to 27) (e.g., Figures 1b and 2).

[8] Air-water flow properties were measured with a series of conductivity probes. Each probe sensor consisted of a sharpened rod (Ø = 0.35 mm) insulated except for its tip and set into the second tubular electrode (Ø = 1.42 mm). The probe output signals were scanned at 10 kHz per channel for 6 s. Data acquisition was triggered manually immediately prior to the flow arrival. At each location x′, one probe (i.e., reference probe) was set on the invert, acting as a time reference, while the other probes were set at different elevations (Figure 2). Each experiment was repeated until sufficient data were obtained at each profile. The displacement of the probes in the direction normal to the invert was controlled by a fine adjustment traveling mechanism. The error in the probe position was less than 0.2 mm and 2 mm in the vertical and horizontal directions respectively. Further information's and the full data set were reported by *Chanson* [2003].

2.1. Signal Processing

[9] Each step was painted with red and white stripes spaced 50 mm apart (Figures 1b and 2). Videotaped movies were analyzed frame-by-frame. The error on the time was less than 1/250 s, and the error on the longitudinal position of the wave front was ±1 cm. In experiments series 1, two video footages were taken for each experiment. In experiments series 2, three video recordings were taken per experiments. All video results are presented in terms of the average over two or three recordings.

[10] In steady flows, the void fraction C is the proportion of time that the probe tip is in the air [e.g., *Chanson*, 1997a, 2002]. In unsteady gas-liquid flows, the processing technique must be adapted. Few studies considered highly unsteady gas-liquid flows [e.g., *Stutz and Reboud*, 2000]. In the present study, the instantaneous void fractions were calculated during a short time interval ΔT such as $\Delta T = \Delta X/U$ where U is the surge front celerity measured with the video cameras and ΔX is the control volume streamwise length (Figure 1a). After preliminary tests, the basic control volume minimum size was set at 70 mm to contain at least 5 to 20 bubbles, that is consistent with the processing technique of *Stutz and Reboud* [2000].

Figure 2. Advancing surge front and conductivity probes. Experiment series 2 ($Q(t = 0+) = 0.075$ m^3/s, $d_o = 0.297$ m, step 10, $h = 0.0715$ m). Advancing surge front just touching the conductivity probe sensors. Looking upstream. See color version of this figure in the HTML.

2.2. Flow Conditions

[11] Prior to the start of each experiment, the recirculation pipe system and convergent intake were emptied. The stepped chute was initially dry. The pump was rapidly started and reached nominal flow rate in 5 s: that is, at least 10 s prior to the water entering the channel. The flow rate $Q(t = 0+)$ was maintained constant until at least 10 s after the surge reached the channel downstream end. Previously, steady flow experiments were conducted in the same channel with a smooth invert and both stepped configurations [*Chanson*, 1997b; *Chanson and Toombes*, 2002]. The steady air-water flow results provided limiting conditions for the present unsteady flow results.

[12] Although the nozzle produced a high-velocity jet flow at the upstream end, strong flow deceleration was measured upstream of the first brink and downstream of the first drop. A comparison between experiments in the present chute and experiments performed on an uncontrolled chute of similar slope and stepped geometry showed that the inflow conditions had little impact, but at the upstream end [*Chanson and Toombes*, 2002]. In the present study, most experiments were focused on the downstream end of the chute (i.e., $x > 10$ m) where the effects of inflow conditions were small.

3. Experimental Results

3.1. Visual Observations

[13] For each experiment, the surge burst out of the nozzle before propagating down the stepped invert. It took about 7 to 11 s to reach the end of the 24 m long flume, depending upon the initial flow rate. Visual observations showed that the surge front propagated as a succession of free-falling nappe and horizontal runoff for all flow rates and geometries. That is, at the end of each step, the advancing surge took off, becoming a free-falling jet which impacted onto the downstream step face. Downstream of nappe impact, the surge flowed horizontally up to the downstream end of the step. Figure 1b illustrates the wave front taking off at the downstream end of a step, while Figures 1a and 2 show the horizontal runoff flow.

[14] The observations emphasized that the wave front was highly aerated, in particular for the larger flow rates (Figures 1b and 2). The photographs highlight further the chaotic nature of wave front, with strong spray, splashing and wavelets. Visually the surge leading edge had a similar appearance to that observed during the Brushes Clough dam spillway tests [*Baker*, 1994], the flash flood propagation through the Glashütte township [*Bornschein and Pohl*, 2003] and laboratory experiments by *Dressler* [1954] above strip roughness elements.

3.2. Surge Front Propagation

[15] The propagation of the surge leading edge was recorded for a range of unsteady flow conditions (Table 1). Dimensionless locations of wave front x_s/d_o are presented in Figure 3 as a function of the dimensionless time $t^* \sqrt{g/d_o}$, where g is the gravity acceleration, x_s is the distance along the pseudo-bottom formed by the step edges measured from the channel upstream end and d_o is a measure of the initial flow rate:

$$d_o = \frac{9}{4} * \sqrt[3]{\frac{Q(t = 0+)^2}{g * W^2}} \quad (6)$$

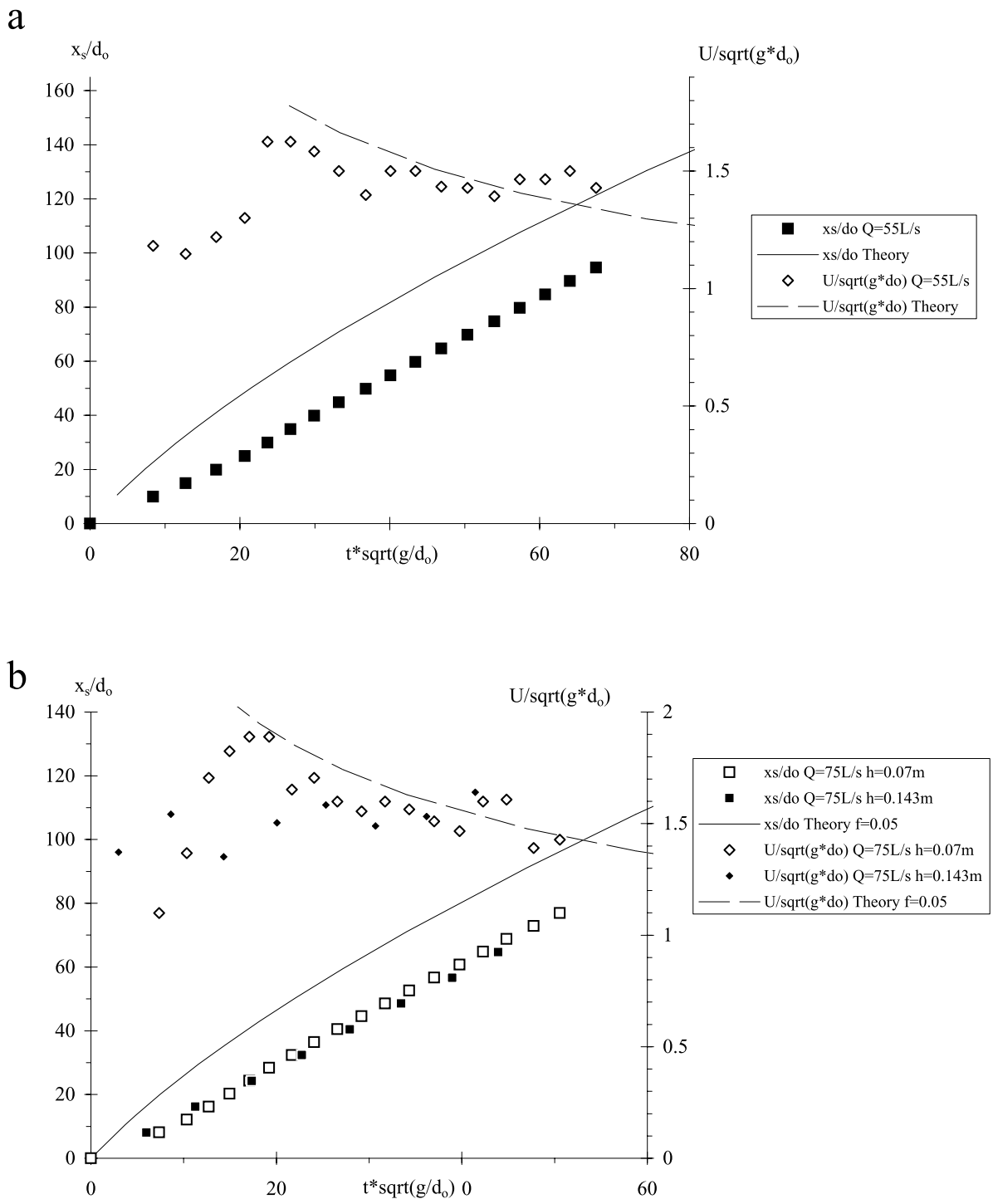

Figure 3. Propagation of the surge front. Dimensionless wave front location x_s/d_o and wave front celerity $U/\sqrt{g*d_o}$. Comparison with *Hunt*'s [1982] theory. (a) $Q(t = 0+) = 0.055$ m^3/s, $d_o = 0.241$ m, h = 0.07 m. (b) $Q(t = 0+) = 0.075$ m^3/s, $d_o = 0.297$ m, h = 0.07, and 0.143 m.

where $Q(t = 0+)$ is the initial flow rate for $t > 0$, and W is the channel width. Physically d_o would be the initial reservoir water depth for a surge propagation down a horizontal initially dry channel [e.g., *Henderson*, 1966; *Montes*, 1998].

[16] Figure 3 presents also dimensionless wave front celerity data $U/\sqrt{g*d_o}$. The wave front celerity was measured over one step length: i.e., the velocity was averaged between one step edge and the next one. For small flow rates ($Q(t = 0+) \leq 0.04$ m^3/s), the wave front celerity U was relatively uniform along the 24 m long chute. For larger discharges, the celerity seemed to increase slightly over the first 4 to 6 steps. Further downstream, a gradual decay was observed. In average, for all flow rates and stepped geom-

etries, the dimensionless wave front celerity at the end of the chute was about

$$\frac{U}{\sqrt{g * d_o}} \approx 1.5 \quad (7)$$

end of 24 m long stepped chute. In the downstream half of the chute, experimental data were compared successfully with *Hunt*'s [1982] theory. For $t^*\sqrt{g/d_o} \geq 35$, a fair agreement with Hunt's theory was achieved assuming an equivalent Darcy-Weisbach friction factor f = 0.05, irrespective of the flow rate and chute configuration (Figure 3). Calculated wave celerity are reported in Figure 3 (dashed line) for $t^*\sqrt{g/d_o} \geq 35$. The predicted wave front locations are also reported (Figure 3, solid line).

[17] In smooth concrete chutes, steady flow friction factors f range typically between 0.01 and 0.03 [e.g., *Henderson*, 1966; *Chanson*, 1999]. In skimming flows down stepped chutes, the equivalent friction factor is about 0.2 [*Chanson et al.*, 2002]. Flow resistance data in step-pool streams yielded similar values, although large wooden debris may induce greater flow resistance [*Mcfarlane and Wohl*, 2003]. Steady flow experiments in the present facility showed f = 0.015 and 0.047 in average for smooth chute and stepped chute flows respectively [*Chanson and Toombes*, 2002]. Present unsteady flow data were in agreement with *Hunt*'s [1982] theory assuming a flow resistance (f = 0.05) that is very close to steady flow experiments with the same invert profile. The result refutes any suggestion that air entrainment at wave front could create an air cushion, inducing some drag reduction. Further the flow resistance estimate $f \sim 0.05$ was found to be independent of step heights (h = 0.07 & 0.143 m) and flow rates for Q(t = 0+) = 0.019 to 0.075 m^3/s.

[18] It should be noted that a comparison with *Hunt*'s [1982] theory is incorrect at the upstream end of the flume since his kinematic wave solution is valid only once the wave front has traveled a distance of more than $4*d_o/S_o$ where d_o is the initial dam height and S_o is the bed slope ($S_o = \sin\theta$). In the present experiments, a comparison with Hunt's theory is valid only for x > 10 to 12 m or $t^*\sqrt{g/d_o} \geq 35$. It may be added that Hunt's theory was developed for smooth inverts. It is believed that the present study is the first application of Hunt's theory to very rough inverts and stepped inverts. This theory provides an exact, analytical development which is an useful modeling tool.

3.3. Wave Front Propagation Along a Single Step

[19] Although Figure 3 suggests an almost linear relationship between surge front location and time, the wave propagation along each step was not smooth. It consisted of nappe take-off at the upstream step edge, free-falling jet, nappe impact and horizontal runoff toward the downstream end of the step. Dimensionless wave front celerity data $U/\sqrt{g*d_o}$ measured on a single step are presented in Figure 4. Figure 4a shows experimental results at one step for three flow rates, while Figure 4b presents experimental data at several steps for one flow rate. In Figure 4, U is the magnitude of the wave celerity: $U = \sqrt{U_x^2 + U_y^2}$, where the subscripts x and y refer to the measured horizontal and vertical celerity component respectively. Although $U = U_x$ downstream of nappe impact, the vertical celerity component must be accounted for in the free-falling nappe. Experiments at two step locations for five flow rates (series 2) demonstrated that the vertical component of wave front celerity U_y satisfied the motion equation and hence basic trajectory equation: i.e., $U_y \propto t' \propto x'$, where t' is the time from take-off and x' is the horizontal distance from the step vertical face. Overall the data highlighted nappe acceleration in the free jet followed by a gradual flow deceleration downstream of nappe impact (Figure 4).

3.4. Surge Front Aeration

[20] Void fractions were recorded at two steps (steps 10 and 16) for three flow rates. On each step, measurements were performed at five locations x' (Figure 1a). Typical void fraction distributions are presented in Figure 5 where void fractions were calculated during a short time interval ΔT such as $\Delta T = \Delta X/U$ where U is the measured surge front celerity and ΔX is the control volume streamwise length. In Figure 5 the vertical axis is the dimensionless vertical distance y/d_o. The legend indicates the location and size of the control volume behind the leading edge of surge front: e.g., 350–735 mm means the control volume located between 350 mm and 735 mm behind the leading edge. In each case, the data are compared with the corresponding steady flow data of *Chanson and Toombes* [2002].

[21] Figure 5 presents data at one location at the end of a step ($x' = 1.0$ m) for two flow rates. Void fraction data showed consistently an increasing surge front thickness with increasing time. The vertical distributions of air contents exhibited a shape somehow close to self-aerated open channel flows [e.g., *Wood*, 1991; *Chanson*, 1997a]. The data suggested consistently maximum flow aeration around $x' = 0.4$ to 0.6 m, corresponding to the nappe impact and spray region, followed by some flow de-aeration further downstream up to the end of the step ($x' = 1.2$ m). Overall the data suggested increasing flow aeration and increasing mean void fraction with increasing initial flow rate Q(t = 0+). The same trend was observed in steady flows down the same facility [*Chanson and Toombes*, 2002].

[22] The distributions of void fractions (Figure 5) demonstrated a strong aeration of the leading edge, especially the first 0.3 to 0.7 m of the wave front flow: i.e., $(t - t_s)*\sqrt{g/d_o} < 1.0$ to 1.2 where t is the time and where t_s is the time of passage of wave front at x'. The finding was clearly seen for all flow rates and steps for $x' \geq 0.4$ m. For example, in Figure 5a, the depth-average void fractions defined between 0 and 90% were C_{mean} = 0.72, 0.45, 0.312 and 0.21 for $(t - t_s)*\sqrt{g/d_o}$ = 0.31, 0.57, 1.6 and $+\infty$ (steady flow) respectively. (That is, for $(t - t_s)$ = 0.05, 0.09, 0.25 s and $+\infty$ respectively.) Another example: in Figure 5b, the depth-average void fractions were C_{mean} = 0.54, 0.22, 0.24 and 0.20 for $(t - t_s)*\sqrt{g/d_o}$ = 0.42, 1.2, 2.0 and $+\infty$ (steady flow). In addition, the data highlighted a distinctive spray region (C > 0.7) extending up to y = 1.5 to 2 * Y_{90}, where Y_{90} is the location where C = 90%. Results in terms of depth-averaged void fractions are detailed in Figure 6, where C_{mean} is defined as

$$C_{mean} = \frac{1}{Y_{90}} * \int_{y=0}^{Y_{90}} C * dy \quad (8)$$

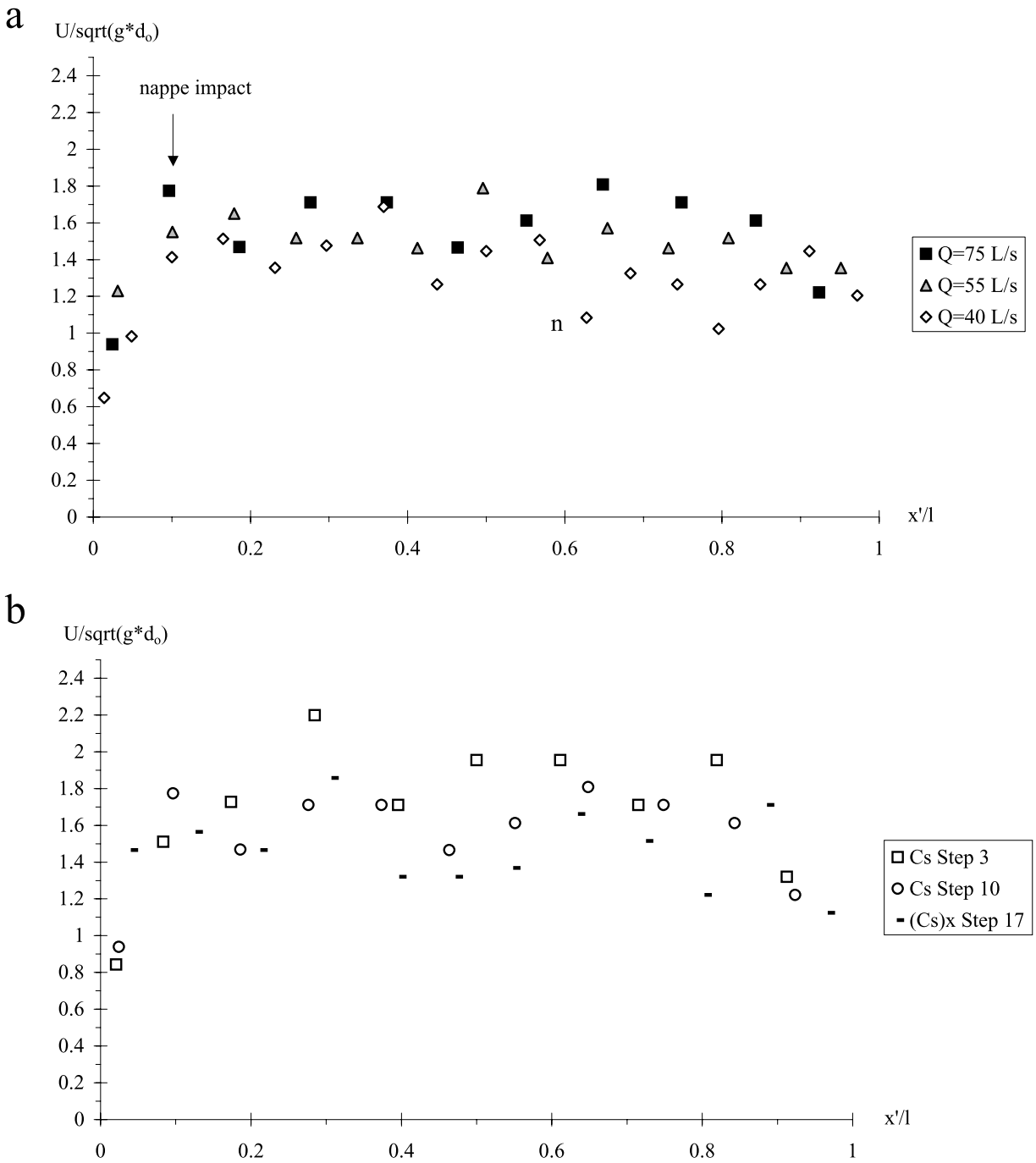

Figure 4. Dimensionless wave front celerity $U/\sqrt{g^*d_o}$ along a single step (series 2, h = 0.07 m). (a) Experimental results at step 10 and three flow rates. (b) Experimental results for Q(t = 0+) = 0.075 m^3/s (d_o = 0.297 m) and three step locations.

In Figure 6 the horizontal axis is the dimensionless time $(t - t_s)*\sqrt{g/d_o}$ with a logarithmic scale. Note that the last data (i.e., $(t - t_s)*\sqrt{g/d_o} > 10$) are the steady flow data The results highlighted a rapid decrease in depth-averaged void fraction with increasing time $(t - t_s)$, especially within the first 0.3 to 0.7 s immediately following the surge front passage at a location x'. For longer times $(t - t_s)$, the depth-averaged properties tended basically the corresponding steady flow conditions.

[23] At the front of surging waters, the void fraction distributions had roughly a linear shape:

$$C = 0.9 * \frac{y}{Y_{90}} \qquad 0.1 < (t - t_s)*\sqrt{g/d_o} < 1.3 \qquad (9)$$

where Y_{90} is the characteristic location where the void fraction equals 0.9. For larger times $(t - t_s)$, the distribution

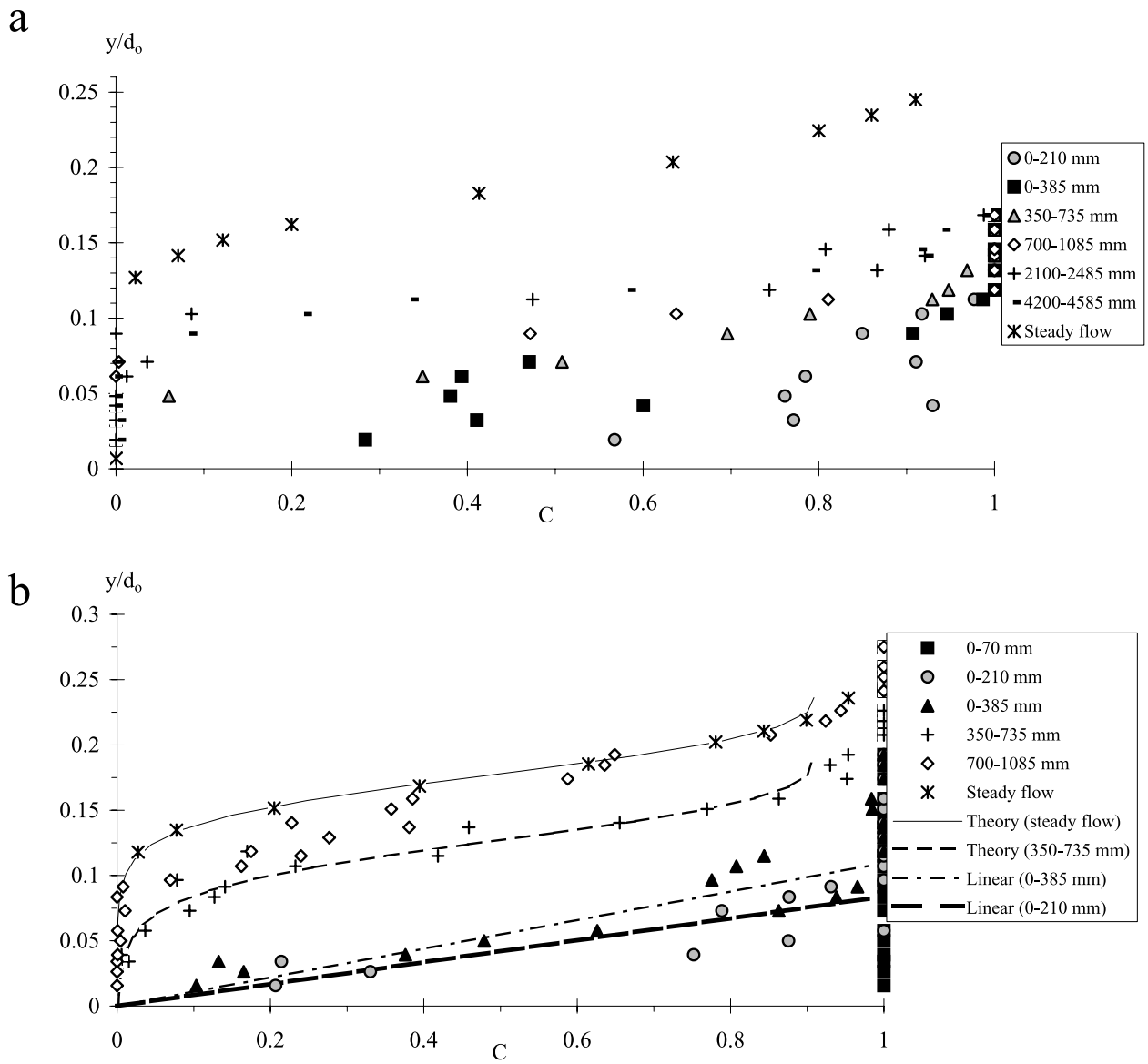

Figure 5. Void fraction distributions behind the leading edge of surge front. Comparison with steady flow data [*Chanson and Toombes*, 2002a]. (a) $Q(t = 0+) = 0.055$ m^3/s, $d_o = 0.241$ m, step 16, $x' = 1$ ($U = 2.14$ m/s, $h = 0.07$ m). ΔX (m) = 0.070, 0.210, 0.385, 0.385, 0.385, 0.385, and 0.385 for 0–70, 0–210, 0–385, 350–735, 700–1085, 2100–2485, and 4200–4585 mm, respectively; $(t - t_s)*\sqrt{g/d_o} = 0.104$, 0.313, 0.573, 1.615, 2.657, 6.826, and 13.08 for 0–70, 0–210, 0–385, 350–735, 700–1085, 2100–2485, and 4200–4585 mm, respectively. (b) $Q(t = 0+) = 0.075$ m^3/s, $d_o = 0.297$ m, $h = 0.07$ m, step 10, $x' = 1.0$ m ($U = 2.61$ m/s, $h = 0.07$ m). Comparison between unsteady data, steady flow data [*Chanson and Toombes*, 2002a], and equations (9) and (10). ΔX (m) = 0.070, 0.210, 0.385, 0.385, 0.385, 0.385, and 0.385 for 0–70, 0–210, 0–385, 350–735, 700–1085, 2100–2485, and 4200–4585 mm, respectively; $(t - t_s)*\sqrt{g/d_o} = 0.077$, 0.231, 0.424, 1.194, 1.965, 5.047, 9.67 for 0–70, 0–210, 0–385, 350–735, 700–1085, 2100–2485, and 4200–4585 mm, respectively.

of air concentration was reasonably well described by a diffusion model developed for steady flows:

$$C = 1 - \tanh^2\left(K'' - \frac{\frac{y}{Y_{90}}}{2 * D_o} + \frac{\left(\frac{y}{Y_{90}} - \frac{1}{3}\right)^3}{3 * D_o}\right) \qquad (10)$$

$$(t - t_s)*\sqrt{g/d_o} > 1.3$$

where K' and D_o are functions of the mean air content only [*Chanson*, 2003]. Equations (9) and (10) are plotted for unsteady and steady flow conditions in Figure 5b. Their theoretical justification is presented in Appendix A.

[24] At the leading edge, the shape of the propagating surge followed closely the wave shape predicted by *Hunt*'s [1984] theory (equation (5)). The characteristic depth Y_{90} satisfied consistently

$$(t - t_s)*\sqrt{\frac{g}{d_o}} \propto \frac{Y_{90}}{(Y_{90})_{steady}} + \mathrm{Ln}\left(1 + \frac{Y_{90}}{(Y_{90})_{steady}}\right) \qquad (11)$$

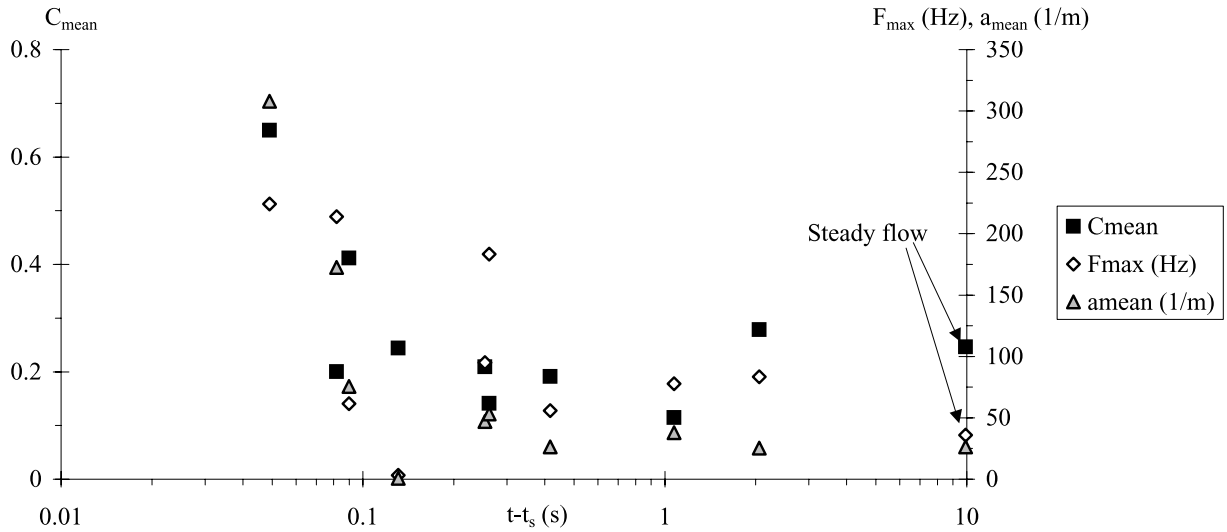

Figure 6. Depth-averaged void fraction C_{mean} behind the surge front as functions of time $(t - t_s)$ for (1) $Q(t = 0+) = 0.040$ m^3/s, $d_o = 0.195$ m, $h = 0.07$ m, step 16, $U = 2.0$ m/s, $x' = 0.8$ m. (2) $Q(t = 0+) = 0.055$ m^3/s, $d_o = 0.241$ m, $h = 0.07$ m, step 16, $U = 2.14$ m/s, $x' = 0.8$ m. (3) $Q(t = 0+) = 0.075$ m^3/s, $d_o = 0.297$ m, $h = 0.07$ m, step 16, $U = 2.43$ m/s, $x' = 0.8$ m.

where $(Y_{90})_{steady}$ is the steady flow characteristic depth where $C = 90\%$. A typical data set is shown in Figure 7 and compared with equation (10).

3.5. Discussion

[25] Void fraction data (e.g., Figure 5) highlighted consistently a major change in void fraction distribution shape for $(t - t_s) * \sqrt{g/d_o} \sim 1.2$ to 1.5. For $(t - t_s) * \sqrt{g/d_o} < 1.2$, the void fraction data exhibited a quasi-triangular distribution, while air concentration profiles had a S-shape for larger times.

[26] Several explanations may be proposed, including a nonhydrostatic pressure field in the leading front of the wave, and some change in air-water flow structure between the leading edge and the main flow associated with a change in rheological fluid properties. Further visual observations seem to suggest some change in gas-liquid flow regime, with some plug/slug flow at the leading edge and a homogenous bubbly flow region behind. There might be also a change in boundary friction regime between the leading edge and the main flow behind. All these mechanisms would be consistent with high-shutter speed movies of leading edge highlighting very dynamic spray and splashing processes.

4. Applications

[27] Present results provide quantitative information on the propagation of surge waves and flash floods down sloping waterways with large roughness. Although developed for smooth channels, *Hunt*'s [1982, 1984] theory may be applicable and a typical Darcy friction factor of $f = 0.05$ is appropriate for flat stepped and step-pool geometries.

[28] The data emphasized further the large air content of the surge leading edge. The result has direct implications in terms of sediment processes at the leading edge of flash

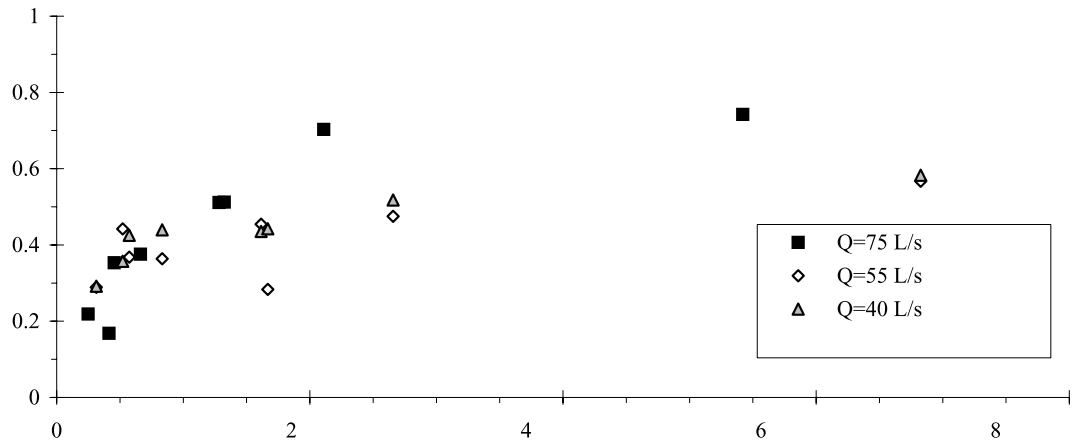

Figure 7. Dimensionless characteristic depth $Y_{90}/(Y_{90})_{steady}$ as function of dimensionless time $(t - t_s)/\sqrt{g/d_o}$. Comparison with equation (11). Step 16, $x' = 1.0$ m, $h = 0.07$ m.

flood and swash zone runup on beaches. The sediment transport rate is a function of the relative sediment density $s = \rho_s/\rho$, where ρ_s is the sediment density and ρ is the fluid density. Known formula of total sediment transport rates yield

$$q_s \propto \frac{1}{(s-1)^n} \quad (12)$$

where q_s is the sediment transport rate per unit width and the exponent n ranges from 0.5 to 3 typically [e.g., *Engelund and Hansen*, 1972; *Graf*, 1971; *Van Rijn*, 1984]. At the surge leading edge, the average fluid density is basically $\rho*(1 - C_{mean})$ where ρ is the clear-water density and C_{mean} is the depth-averaged void fraction (e.g., Figure 6). For a mean void fraction 50%, the term $(s - 1)$ equals 4.3 (compared to 1.65 in clear-water) for quartz particles. Equation (12) implies that, at the surge leading edge, the flow aeration, and the lesser relative sediment density, could cause a drastic reduction in transport rate. Considering that the Shields parameter is proportional to $(s - 1)^{-1}$ and that the particle settling velocity is proportional to $(s - 1)$, a lesser buoyancy, all other parameters being identical, might induce lesser sediment bed load and suspension motion.

[29] The above reasoning is based upon the effects of flow aeration with all parameters, including turbulence, being identical. It is off course acknowledged that the surge front is highly turbulent [e.g., *Capart and Young*, 1998]. In any case, the large amount of air entrainment (i.e., "white waters") observed at the surge leading edge increases the relative density of sediment particles and might affect the sediment motion.

5. Conclusion

[30] New flash flood surge experiments were conducted systematically down a 24-m long waterway with a stepped bottom. Experimental results demonstrated that the surging waters propagated as a succession of free-falling nappe, nappe impact and horizontal runoff on each step for all investigated flow conditions. Visual observations highlighted the chaotic nature of the advancing flow associated with strong aeration of the leading edge. Observations of surge front propagation showed some flow deceleration in the downstream half of the channel. The celerity data were successfully compared with *Hunt*'s [1982, 1984] dam break wave theory assuming a Darcy-Weisbach friction factor f = 0.05 independently of flow rates and step heights. The finding suggests that Hunt's development may provide an useful prediction tool in rough sloping channels and waterways.

[31] Unsteady void fraction measurements were performed in the surge front. The results demonstrated quantitatively strong aeration of the leading edge, although the flow properties tended rapidly toward steady flow characteristics. Void fraction distributions showed a marked change in shape for $(t - t_s)*\sqrt{g/d_o} \sim 1.3$. Several explanations were proposed, suggesting some major change in air-water flow properties between the wave leading edge and the surging waters behind. The strong aeration of the surge front might have some impact on sediment motion near the leading edge, because the sediment relative density is inversely proportional to the air and water fluid density. This point must be further investigated in movable-bed channels, although a study of three-phase flow (air, water, solid) is challenging.

Appendix A: Void Fraction Distributions in Supercritical Open Channel Flow

[32] In supercritical open channel flows, free-surface aeration or "white waters" occurs when turbulence acting next to the free surface is large enough to overcome both surface tension for the entrainment of air bubbles and buoyancy to carry downwards the bubbles. Assuming a homogeneous air-water mixture for $0 < C < 90\%$, the advective diffusion of air bubbles may be analytically predicted. At uniform equilibrium, the continuity equation for air in the air-water flow yields

$$\frac{\partial}{\partial y}\left(D_t * \frac{\partial C}{\partial y}\right) = \cos\theta * \frac{\partial}{\partial y}(u_r * C) \quad (A1)$$

where C is the void fraction, D_t is the air bubble turbulent diffusivity, u_r is the bubble rise velocity, θ is the channel slope and y is measured perpendicular to the mean flow direction. The bubble rise velocity in a fluid of density $\rho*(1 - C)$ equals:

$$u_r^2 = \left[(u_r)_{Hyd}\right]^2 * (1 - C)$$

where $(u_r)_{Hyd}$ is the rise velocity in hydrostatic pressure gradient [*Chanson*, 1995, 1997]. A first integration of the continuity equation for air leads to

$$\frac{\partial C}{\partial y} = \frac{1}{D'} * C * \sqrt{1 - C} \quad (A2)$$

where $y' = y/Y_{90}$, and Y_{90} is the location where C = 0.90. D′ is the ratio of the air bubble diffusion coefficient to the rise velocity component normal to the flow direction times the characteristic transverse dimension of the shear flow:

$$D' = \frac{D_t}{(u_r)_{Hyd} * \cos\theta * Y_{90}}$$

Assuming a bubble diffusivity distribution such as

$$D' = \frac{C * \sqrt{1 - C}}{0.9} \quad (A3)$$

the analytical solution of equation (A2) is

$$C = 0.9 * \frac{y}{Y_{90}} \quad (A4)$$

and the depth-averaged void fraction equals $C_{mean} = 0.45$. If a bubble diffusivity distribution satisfies

$$D' = \frac{D_o}{1 - 2 * \left(\frac{y}{Y_{90}} - \frac{1}{3}\right)^2} \quad (A5)$$

the analytical solution of the advective diffusion equation yields

$$C = 1 - \tanh^2\left(K' - \frac{\frac{y}{Y_{90}}}{2 * D_o} + \frac{\left(\frac{y}{Y_{90}} - \frac{1}{3}\right)^3}{3 * D_o}\right) \quad (A6)$$

where D_o and K' are functions of the depth-averaged air content only:

$$K' = K^* + \frac{1}{2 * D_o} - \frac{8}{81 * D_o}$$

$$\text{with } K^* = \tanh^{-1}\left(\sqrt{0.1}\right) = 0.32745015\ldots$$

$$C_{mean} = 0.7622*(1.0434 - \exp(-3.614*D_o))$$

Equations (A4) and (A6) were first derived by *Chanson and Toombes* [2001].

Notation

- C void fraction, or air content, defined as the volume of air per unit volume of air and water.
- C_{mean} depth averaged air content defined in terms of Y_{90}, $C_{mean} = \frac{1}{Y_{90}} * \int_{y=0}^{Y_{90}} C * dy$.
- D_t air bubble turbulent diffusivity (m^2/s).
- D' dimensionless air bubble diffusivity (Appendix A).
- D_o dimensionless coefficient (Appendix A).
- d_s dam break wave front thickness (m).
- d_o equivalent surge reservoir depth (m), $d_o = \frac{9}{4} * \sqrt[3]{\frac{Q^2}{g*W^2}}$.
- d_o initial reservoir height (m).
- f Darcy-Weisbach friction factor.
- g gravity acceleration (m/s^2).
- h vertical step height (m).
- K' dimensionless integration constant (Appendix A).
- K^* dimensionless integration constant (Appendix A).
- l horizontal step length (m).
- $Q(t = 0+)$ initial water discharge (m^3/s).
- q_s sediment transport rate per unit width (m^2/s).
- t time (s), usually $t = 0$ when $x_s = 0$.
- t' time (s) measured from nappe take-off.
- U surge front celerity (m/s).
- u_r bubble rise velocity (m/s).
- u_r bubble rise velocity (m/s) in hydrostatic pressure gradient.
- V_H uniform equilibrium flow velocity)m) for a water depth d_o.
- S_o bed slope, $S_o = \sin\theta$.
- s sediment particle relative density.
- W channel width (m).
- x longitudinal flow distance (m) measured horizontally from the channel intake.
- x' horizontal distance (m) measured from the vertical step height.
- x_s wave front coordinate (m).
- x_s' wave front position (m) measured from the vertical step height.
- Y_{90} characteristic distance (m) where $C = 0.9$.
- y vertical direction (m) normal to the channel bed.
- ΔT integration time (9 s).
- ΔX control volume streamwise length (m).
- θ channel slope.
- ρ water density (kg/m^3).
- ρ_s sediment particle density (kg/m^3).
- Ø diameter.

Subscripts

- steady steady flow conditions.
- x horizontal direction component.
- y vertical direction component.

[33] **Acknowledgments.** The author thanks his students C. H. Lim, C. G. Sim, C. C. Tan and Y. W. Tan for their help and assistance. He acknowledges the assistance of L. Toombes (Australia). Helpful comments from the reviewers and Associate Editor are acknowledged.

References

Baker, R. (1994), Brushes Clough Wedge block spillway, *Progress Rep. 3*, *SCEL Proj. Rep. SJ542-4*, 47 pp., Univ. of Salford, Salford, U. K., Nov.

Bornschein, A., and R. Pohl (2003), Dam break during the flood in Saxon/Germany in August 2002, in *30th IAHR Biennial Congress, Thessaloniki, Greece*, vol. C2, edited by J. Ganoulis and P. Prinos, pp. 229–236, IAHR Congr. Organ., Thessaloniki, Greece.

Capart, H., and D. L. Young (1998), Formation of a jump by the dam-break wave over a granular bed, *J. Fluid Mech.*, *372*, 165–187.

Chanson, H. (1995), Air bubble diffusion in supercritical open channel flow, in *Proceedings of 12th Australasian Fluid Mechanics Conference AFMC*, vol. 2, edited by R. W. Bilger, pp. 707–710, Univ. of Sydney, Sydney, Australia.

Chanson, H. (1997a), *Air Bubble Entrainment in Free-Surface Turbulent Shear Flows*, 401 pp., Academic, San Diego, Calif.

Chanson, H. (1997b), Air bubble entrainment in open channels: Flow structure and bubble size distributions, *Int. J. Multiphase Flow*, *23*, 193–203.

Chanson, H. (1999), *The Hydraulics of Open Channel Flows: An Introduction*, 512 pp., Butterworth-Heinemann, Woburn, Mass.

Chanson, H. (2001), *The Hydraulics of Stepped Chutes and Spillways*, 418 pp., A. A. Balkema, Brookfield, Vt.

Chanson, H. (2002), Air-water flow measurements with intrusive phase-detection probes: Can we improve their interpretation?, *J. Hydraul. Eng.*, *128*, 252–255.

Chanson, H. (2003), Sudden flood release down a stepped cascade. Unsteady air-water flow measurements. Applications to wave run-up, flash flood and dam break wave, *Rep. CH51/03*, 142 pp., Dep. of Civ. Eng., Univ. of Queensland, Brisbane, Australia, Jan.

Chanson, H., and L. Toombes (2001), Strong interactions between free-surface aeration and turbulence down a staircase channel, paper presented at 14th Australasian Fluid Mechanics Conference, Adelaide Univ., Adelaide, Australia.

Chanson, H., and L. Toombes (2002), Energy dissipation and air entrainment in a stepped storm waterway: An experimental study, *J. Irrig. Drain. Eng.*, *128*, 305–315.

Chanson, H., Y. Yasuda, and I. Ohtsu (2002), Flow resistance in skimming flows and its modelling, *Can. J. Civ. Eng.*, *29*, 809–819.

Dressler, R. F. (1952), Hydraulic resistance effect upon the dam-break functions, *J. Res. Natl. Bur. Stand.*, *49*, 217–225.

Dressler, R. (1954), Comparison of theories and experiments for the hydraulic dam-break wave, paper presented at Assemblée Générale, Intl. Assoc. of Sci. Hydrol., Rome, Italy.

Engelund, F., and E. Hansen (1972), *A Monograph on Sediment Transport in Alluvial Streams*, 3rd ed., 62 pp., Teknisk Forlag, Copenhagen.

Graf, W. H. (1971), *Hydraulics of Sediment Transport*, McGraw-Hill, New York.

Henderson, F. M. (1966), *Open Channel Flow*, MacMillan, Old Tappan, N. J.
Hunt, B. (1982), Asymptotic solution for dam-break problems, *Proc. Hydraul. Div. Am. Soc. Civ. Eng.*, *108*, 115–126.
Hunt, B. (1984), Perturbation solution for dam break floods, *J. Hydrol. Eng.*, *110*, 1058–1071.
Khan, A. A., P. M. Steffler, and R. Gerard (2000), Dam-break surges with floating debris, *J. Hydraul. Eng.*, *126*, 375–379.
Macfarlane, W. A., and E. Wohl (2003), Influence of step composition on step geometry and flow resistance in step-pool streams of the Washington Cascades, *Water Resour. Res.*, *39*(2), 1037, doi:10.1029/2001WR001238.
Montes, J. S. (1998), *Hydraulics of Open Channel Flow*, Am. Soc. of Civ. Eng., Reston, Va.
Nsom, B., K. Debiane, and J. M. Piau (2000), Bed Slope Effect on the Dam Break Problem, *J. Hydraul. Res.*, *38*, 459–464.
Ré, R. (1946), Etude du Lacher Instantané d'une Retenue d'Eau dans un Canal par la Méthode Graphique, *Houille Blanche*, *1*, 181–187, 5 plates.
Schnitter, N. J. (1994), *A History of Dams: The Useful Pyramids*, A. A. Balkema, Brookfield, Vt.
Smith, N. (1971), A *History of Dams*, Chaucer, London.
Stutz, B., and J. L. Reboud (2000), Measurements within unsteady cavitation, *Exp. Fluids*, *29*, 545–552.
Van Rijn, L. C. (1984), Sediment transport, part III: Bed forms and alluvial roughness, *J. Hydraul. Eng.*, *110*, 1733–1754.
Wood, I. R. (1991), *Air Entrainment in Free-Surface Flows*, *IAHR Hydraul. Struct. Design Manual*, vol. 4, 149 pp., A. A. Balkema, Brookfield, Vt.

H. Chanson, Fluid Mechanics, Hydraulics and Environmental Engineering, Department of Civil Engineering, University of Queensland, Brisbane QLD 4072, Australia. (h.chanson@uq.edu.au)